Check for updates

Detection of limited-energy α particles using CR-39 in laser-induced $p - {}^{11}B$ reaction

Putong Wang[1,2], Xiangai Deng[3], Zhiguo Ma[3], Changbo Fu[3]*, Lulin Fan[2,4], Qingsong Wang[2,4], Jiancai Xu[4], Tongjun Xu[4], Liangliang Ji[4]*, Baifei Shen[5], Yancheng Liu[1], Xiguang Cao[1,6], Guoqiang Zhang[1,6]* and Yugang Ma[1,2,3]*

[1]Shanghai Institute of Applied Physics, Chinese Academy of Sciences, Shanghai, China, [2]University of Chinese Academy of Sciences, Beijing, China, [3]Key Laboratory of Nuclear Physics and Ion-Beam Application (MOE), Institute of Modern Physics, Fudan University, Shanghai, China, [4]State Key Laboratory of High Field Laser Physics, CAS Center for Excellence in Ultra-intense Laser Science, Shanghai Institute of Optics and Fine Mechanics(SIOM), Chinese Academy of Sciences (CAS), Shanghai, China, [5]Shanghai Normal University, Shanghai, China, [6]Shanghai Advanced Research Institute, Chinese Academy of Sciences, Shanghai, China

Due to the harsh radiation environment produced by strong laser plasma, most of the detectors based on semiconductors cannot perform well. So, it is important to develop new detecting techniques with higher detection thresholds and highly charged particle resolution for investigating nuclear fusion reactions in laser-plasma environments. The Columbia Resin No. 39 (CR-39) detector is mainly sensitive to ions and insensitive to the backgrounds, such as electrons and photons. The detector has been widely used to detect charged particles in laser-plasma environments. In this work, we used a potassium−ethanol−water (PEW) etching solution to reduce the proton sensitivity of CR-39, by raising the detection threshold for the research of laser-induced ${}^{11}B(p, \alpha)2\alpha$ reaction. We calibrated the $3-5$ MeV α particles in an etching condition of 60°C PEW-25 solution (17% KOH + 25%C_2H_5OH + 58%H_2O) and compared them with the manufacturer's recommended etching conditions of 6.25 N NaOH aqueous solution at 98°C in our laser-induced nuclear reaction experiment. The results indicate, with the PEW-25 solution, that CR-39 is more suitable to distinguish α tracks from the proton background in our experiment. We also present a method to estimate the minimum detection range of α energy on specific etching conditions in our experiment.

1 Introduction

Nuclear fusion reactions play a crucial role in astrophysics because they are not only important for the power of stars in the sky but also indispensable for the synthesis of the elements in the Universe [1–6]. Additionally, it is the core area of research for developing fusion power plants in the future. Nuclear reactions can now be produced in a plasma environment with the recent rapid development of ultrashort, high-intensity laser technology [7, 8]. In such experiments, single or multiple laser beams deposit energy into a target (flat or structured) within a split second and in a tiny volume. The target will be heated and compressed. A hot and dense plasma is then created, which is substantial for the

nuclear fusion reactions [9]. Investigating these reactions in the plasma environment generated by high-intensity laser in the laboratory is meaningful because this environment is similar to that of nuclear astrophysics [10,11] and the fusion reactors in the future. Among the nuclear reactions in the plasma, $^{11}B(p, \alpha)2\alpha$ seems to draw most attention for the purpose of clean energy [12–17].

Due to the strong electromagnetic pulse (EMP) radiation and multiple ions generated by the high-intensity laser, laser-plasma experiments involve more difficult and complex particle-discrimination tasks than traditional nuclear reaction experiments performed at accelerators. A wide range of energy resolution and good detection efficiency is necessary for detectors to distinguish between various ion species in a laser-plasma environment. The detectors should be tough enough to tolerate the strong radiation. Among these detectors, the Time-of-Flight (TOF) detector seems to be working well now for neutrons [18–20], charged particles [21, 22], and delayed gammas or X-rays [23, 24]. The TOF detectors are mainly based on fast scintillators, such as plastic, liquid scintillators, and SiC. They could recover in a very short time (several ns to tens of ns) back from EMP pulse to detect the following particles. Another type of detector working well in a harsh environment is the radiochromic film dosimetry (RCF) [25] or imaging plate (IP) [26–29]. They record the radiation dose (color or delayed light) in the film and can work together with some electric or magnetic field to record the information of the particles. In this work, we attempt to use the CR-39 track detector to detect α particles using a new etching solution.

Solid-state nuclear track detectors (SSNTDs) can be used to detect even a single ion. Typical SSNTD materials include CR-39, cellulose nitrate (CN), and polycarbonate (PC) [30–32]. The chemical name of Columbia Resin No. 39 (CR-39) is poly-allyl-diglycol-carbonate($C_{12}H_{18}O_7$). It is a high-grade plastic with very good light transmission, a refractive index close to 1.5, a density of 1.3 g/cm³ and can be safely used at temperatures up to 100°C [33,34]. CR-39 detectors do not respond to EMPs and X-rays. Charged particles, such as protons, deuterons, α particles, and heavy ions, can be detected using CR-39 detectors [35]. CR-39 provides the absolute number of particles with 100% detection efficiency if these incident particles deposit enough energy and the incident angle is larger than critical. When a charged particle enters CR-39, it breaks the bonds of the molecular chain and leaves a trail of damage full of free radicals along its path. Radiation damage occurs, and the area of radiation damage is called the latent track. Using a microscope, the latent track information can be read after chemical etching creates a conical opening with a diameter of a few microns called a track. During the etching process, the bulk etch rate (V_B) and track etch rate (V_T) are used to describe the growth of the track. V_B and V_T depend on the SSNTD material and etching solution, and V_T depends on the incident ions' linear energy transfer (LET). The amount of local damage along the track is indirectly related to the loss of energy per unit path length, and the length of the latent track indicates the range of the particles in the plastic. The track position is where charged particles' incidence and the average track diameter will depend on the incident energy and etching chemistry.

It is known that etching CR-39 detectors in 6.25 N NaOH aqueous solution at 70°C and 98°C is appropriate [38–41]. The etching response of CR-39 bombarded by α with energies varying up
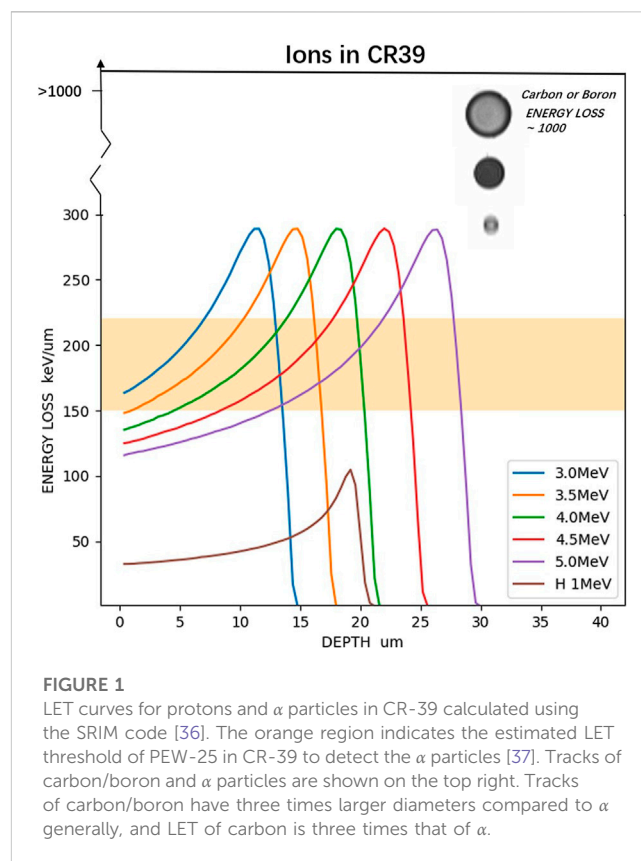

FIGURE 1
LET curves for protons and α particles in CR-39 calculated using the SRIM code [36]. The orange region indicates the estimated LET threshold of PEW-25 in CR-39 to detect the α particles [37]. Tracks of carbon/boron and α particles are shown on the top right. Tracks of carbon/boron have three times larger diameters compared to α generally, and LET of carbon is three times that of α.

to 7.7 MeV has already been studied under specific etching conditions [41–46]. In $p - ^{11}B$ reaction experiment, the main particles in plasma and reaction products are proton (p), boron ($^{11}B, ^{10}B$), carbon (C), and α particles (α), as shown in Eq. 1. It is hard to discriminate the ions in these types of experiments with the solution of NaOH because the background from accelerated ions, such as proton or carbon, has a large range of energy, and their tracks will lead to different, overlapping diameters. Even more complicated is the over-etched state, which involves ions of different energies and etching times. In this case, all the tracks are similar and can no longer be differentiated. Even with an aluminum foil with a thickness of 5 or 10 microns to effectively stop the majority of the low-energy carbon and boron ions from the laser-induced plasma, the energetic ions can still penetrate the foil, leaving their tracks in the following detectors, which will mix with those tracks of α particles with energy between 3 and 5 MeV from the nuclear fusion. Therefore, it is important to raise the detection threshold of ions to suppress background tracks produced by protons and achieve a better charge resolution:

$$p + {}^{11}B \rightarrow 3\alpha + 8.6 MeV. \tag{1}$$

An approach to raise the detection threshold of CR-39 is the use of a copolymer resin of CR-39 and diallyl phthalate (DAP) [47, 48]. Although the CR-39–DAP detector is a candidate for the detection of heavy ions, charge resolution deteriorates due to the extremely rough surface conditions that result from chemical etching. This will be much more serious in the condition of laser plasma. Another approach to raising the detection threshold of CR-39 is to use a
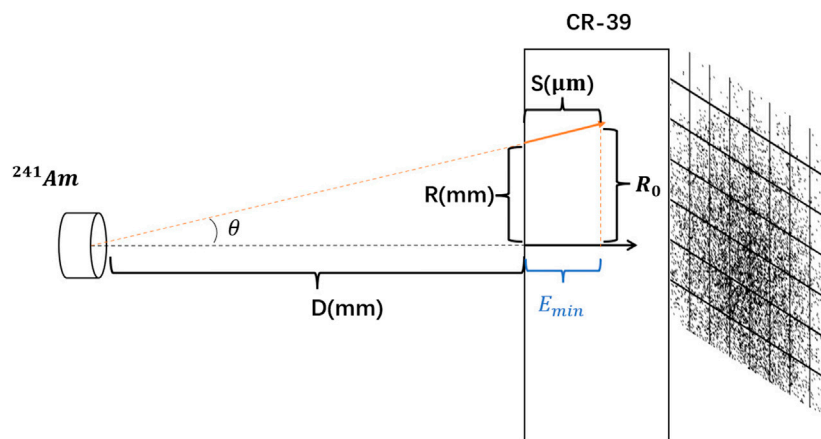
FIGURE 2
Experimental setup used to irradiate CR-39 samples with α particles. E_{min} is the estimated range of α energy.

potassium–ethanol–water (PEW) solution for the etching process. It is valuable to use PEW solutions (17% KOH + χ%C_2H_5OH +(83-χ)%H_2O), with the mass percentage the same as that in the paper for the discrimination of the proton and α particle. It is known that the PEW solution can desensitize the track registration sensitivity of CR-39, and the desensitization of sensitivity is more effective for low-LET particles. The discrimination of proton and α particles is the presence or absence of tracks rather than the diameter of tracks with the PEW solution method. The combination of CR-39 and PEW solution has been used to study the ions, and the great majority of proton tracks are desensitized and disappear [37, 49–51]. This method permits the discrimination of ions other than protons. Figure 1 illustrates the energy loss of α and proton in CR-39. Using the combination of CR-39 and the PEW solution to discriminate small numbers of secondary ions of interest from large numbers of background primary protons would be valuable for laser-plasma research.

In this experiment, we tested different energies of α, which were emitted by an ^{241}Am isotope. A solution of PEW-25 [25%C_2H_5OH] at a temperature of 60°C recommended by Ref. [37] was used to etch CR-39. In order to detect the secondary α particles of the $p - ^{11}B$ reaction in the background of laser plasma, a new approach to obtain the track information and its energy range of incident α at an etching time of 30–60 min was used.

2 Experiments setting

Sheets of CR-39 (TASTRAK@, United Kingdom) with sizes of 25 mm × 25 mm × 1.5 mm were used in this experiment. The manufacturer's recommended α etching conditions are 6.25 N NaOH at 98°C or 70°C. However, it is invalid in a specific laser-induced nuclear reaction environment. As mentioned in the introduction, CR-39 was etched in the PEW-25 solution at 60°C for 30–90 min to discriminate the proton and the α particle in the $p - ^{11}B$ reaction experiment. The temperature of 60°C was selected to avoid the evaporation of ethanol. Under these etching conditions, the LET threshold for CR-39 with

PEW-25 was estimated to be 150–220 keV/um, as shown in Figure 1, and the protons cannot be detected.

Figure 2 shows the experimental setup used for direct irradiation with α particles. To generate α with different energies, an ^{241}Am isotope emitting 5.40 MeV α particles with an intensity of 7.197 kBq was used in the different distances (D) between the isotope source and CR-39 in the open air so that the incident energy of α can be varied. The kinetic energy of α was 5.40 MeV at the source surface and decreased with an increase in the air gap distance. The air gap distance between the detector and source, resulting in different α energies, has been researched by previous studies. The surface of CR-39 was irradiated with the α at the energy of 3.00 MeV (D = 24.5 mm), 4.00 MeV (D = 16.4 mm), and 5.00 MeV (D = 6.2 mm) [41]. CR-39 was covered with an aluminum foil of 5 or 10 microns to simulate CR-39 in the laser-driven nuclear reaction experiment that could reduce the influence of heavier ions with low kinetic energy. By controlling the irradiation time, the number of particles incident to CR-39 was controlled to be less than 10^6 cm^{-2}.

Before chemistry etching, the PEW solution was heated to 60°C. Then, the irradiated CR-39 was clamped with a tetrafluoroethylene (C_2F_4) basket to ensure it was vertical and fully etched. After etching, the CR-39 detector was first washed in 500 mL of carbonic acid solution to neutralize alkaline substances. Then, it was washed in 500 mL of deionized water for cooling. After an appropriate chemical etching treatment, the damaged pit induced by the ionized particles in the CR-39 solid-state track detector can be visualized under an optical microscope. The track information of α was measured using an automatic track image analyzer. Information about the track position, track diameter, major axis, minor axis, and other track information was recorded by the TASLImage radon and neutron dosimetry system from the manufacturer (TASL) of CR-39. These tracks' information could be used to identify the type of particle. They mainly depend on the ion energy, ion mass, ion charge, and etching condition. TASLImage software can only record the track diameter between 3 and 40 microns so that some background noise can be removed.
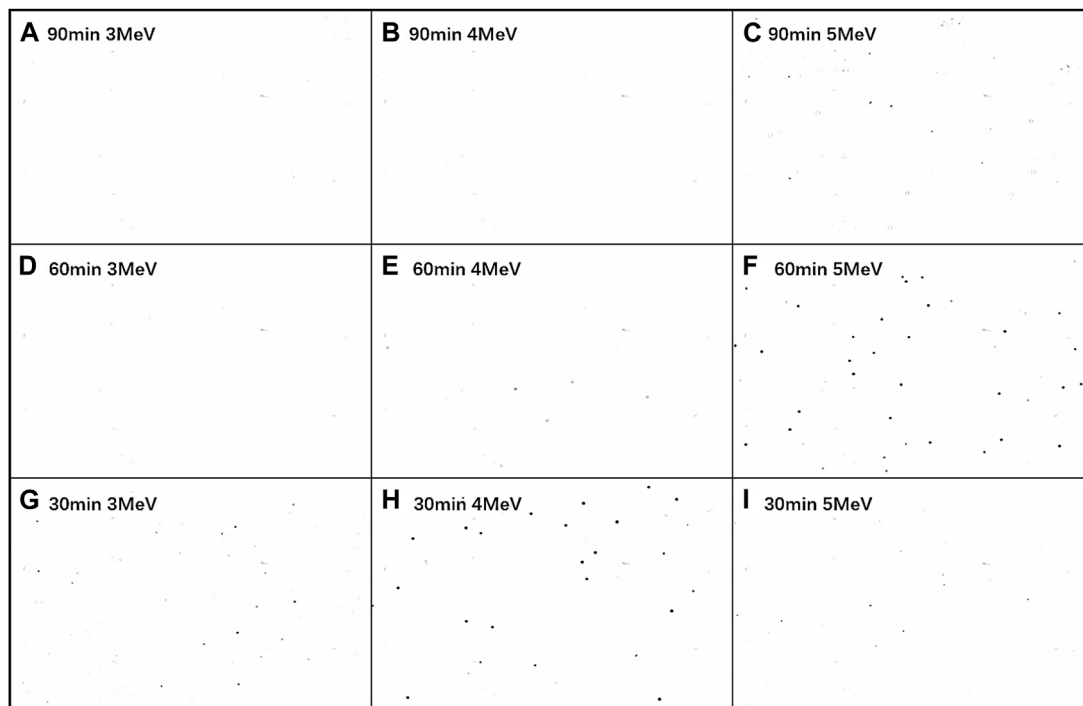
FIGURE 3
Etched CR-39 surfaces after irradiation with **(A)**, **(D)**, **(G)** 3.00 MeV; **(B)**, **(E)**, **(H)** 4.00 MeV; **(C)**, **(F)**, **(I)** 5.00 MeV covered with 5-μm aluminum foil in different etching times.

3 Results and discussion

3.1 CR-39 irradiated by different energies of α particles and covered with 5-μm aluminum foil

The calibration of CR-39 was studied under different etching conditions, before this study [41]. The etching responses are different due to different CR-39 manufacturers, production series in factor, and even the condition in the detector storage history and age. Therefore, CR-39 must be calibrated before experiments.

To determine the optimal etching time to discriminate 3–5 MeV α tracks, CR-39 was irradiated by energies of α covered with 5 μm aluminum foil, as shown in Figure 3. When the etching time was 90 min and CR-39 was covered with 5-μm aluminum foil, only 5.00-MeV α particle tracks could be seen, and only shallow (and hollow) etch pits were actually produced. These etch pits might have been generated by a 5.00 MeV α particle, as shown in Figure 3C. That indicates that the thickness of the layer removed by the PEW-25 solution is larger than the particle path length of 3.00-and 4.00-MeV α particles under etching conditions of 60°C, 90 min, and 5 μm aluminum foil. The 5.00-MeV α particles would penetrate the CR-39 a little shallower than the etched depth.

Figures 3D, E, F show the surfaces of the etched CR-39 after irradiation with 3.00-, 4.00-, and 5.00-MeV α particles, respectively. As shown in Figure 3F, tracks were clearly observed after irradiation with the 5.00-MeV α particles. In contrast, no tracks or etch pits can be seen in Figure 3D with 3.00-MeV α particles. The 4.00-MeV α

particle tracks can be seen; they have a lower grey level than the tracks irradiated by the 5.00-MeV α particles, as shown in Figures 3E, F. The removed layer length of CR-39 under etching conditions of 60°C, 60 min, and 5.0-μm aluminum foil is estimated between the Bragg peak of 4.00-MeV and 5.00-MeV α, and at the end of the Bragg peak, the LET of 4.00-MeV α is fortunately close to the orange region in Figure 1 in this etching condition.

The surfaces of the etched CR-39 after irradiation with 3.00-, 4.00-, and 5.00-MeV α particles are shown in Figures 3G, H, I. Tracks irradiated by 3.00-MeV α particles have an appearance similar to those of tracks irradiated by 4.00-MeV α particles on the etching time of 60 min (e), with a lower grey level than tracks irradiated by 4.00-MeV α particles, as shown in Figures 3G, H. In comparison to the etching time of 60 min, the removed layer length of CR-39 on the etching time of 30 min is estimated to be between the Bragg peak of 3.00- and 4.00-MeV α. Therefore, the tracks were clearly observed after irradiation with the 4.00-MeV α particles. The LET of 5.00-MeV α particles at this etching length has just begun to rise to the LET threshold of PEW-25 so that 5.00-MeV α particles are almost not producing tracks or have a few tracks, as shown in Figure 3I.

As the calibration of CR-39 with PEW-25 solution and 5-μm aluminum foil, an etching time of 30–90 min is appropriate to detect 3–5 MeV α of the $p - {}^{11}B$ reaction. As shown in Figure 3, the states shown in (G), (E), and (C) are similar, where the removed length is a little longer than the depth of the Bragg peak. The states in (F) and (H) are similar, and one could imagine that conditions of 90 min and 6.0 MeV would have an analogous appearance. The etch rate could
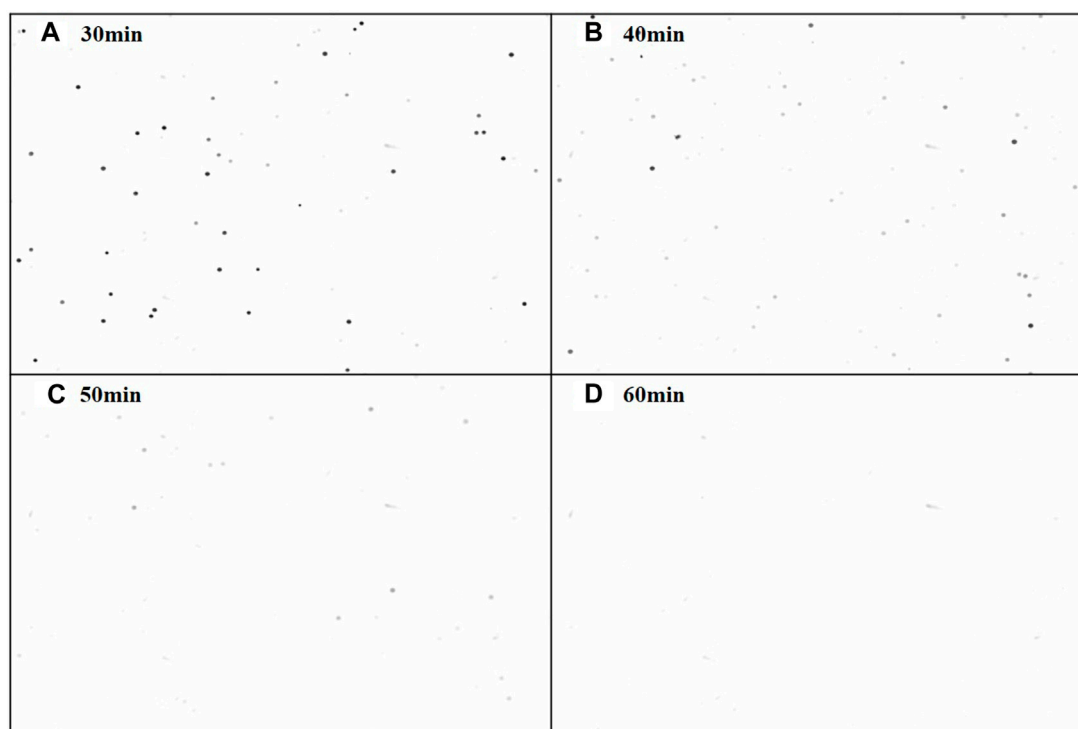
FIGURE 4
Etched CR-39 surfaces after irradiation with 5.00-MeV alpha particles covered with 10-μm aluminum foil. **(A–D)** shown different etching times of CR-39.

be estimated as around 7.0 μm/30 min, which is almost twice that in Ref. [37], 7.5 μm/h. This may be due to different manufacturers of CR-39.

3.2 CR-39 irradiated by 5.00-MeV α particles and covered with 10-μm aluminum foil

In the environment of laser-induced plasma, some heavy ions (e.g., B, C, and N) may be accelerated to energies high enough to penetrate the 5-μm or thicker aluminum foil. Their LET is much higher than the LET threshold of PEW-25 for α particles, leaving tracks of different diameters in a wide range (even >30 μm). The tracks smaller than 10 μm produced by the particles far from the Bragg peak are likely to be confused with tracks produced by the α particles around the Bragg peak. Moreover, a large number of tracks (or etch pits) with a large diameter will disturb the focus of the optical microscope, so a mistake in the record system may happen. For this case, a thicker aluminum foil will reduce the influence of energetic heavy ions in laser-induced nuclear reaction experiments.

Figures 4A–D show the surface of etched CR-39 covered with 10-μm aluminum foil after irradiation with 5.00-MeV α particles, and etching times are 30, 40, 50, and 60 min, respectively. No tracks or etch pits can be seen in Figure 4D with an etching time of 60 min. As the etching time increases, the grey level of the tracks decreases until they disappear in the optical microscope. To reduce the impact of those energetic heavy ions $^{11}B, ^{12}C$ in a laser-induced $p - ^{11}B$

reaction, the etching time is limited between 30 and 40 min with CR-39 covered by a 10-μm aluminum foil.

3.3 An approach to estimate the minimum detection range of α energy

One approach could estimate the energy according to the depth of the α penetrating the CR-39 detector. The diameter of α tracks in the PEW solution is much smaller than that in the NaOH solution. It will disappear quickly when the depth is deeper than the Bragg peak. This provided a method to estimate the minimum detection range of α energy and an etch rate of 3.3 μm/10 min from the data estimated by E_{min} corresponding minimum depth. As shown in Figure 2, without a collimator setting between the CR-39 detector and ^{241}Am isotope, the distribution of tracks on the CR-39 surface will cover a big range with radii around 2.5 mm. For those outer tracks, due to their much longer journey in the air, the α particles will have smaller energy and a more swallow depth in CR-39. Therefore, one can estimate the minimum energy detection ability of CR-39 for α particles from the outer tracks. As shown in Figure 2, R_0 is the radius of distribution, and the track on the circle's edge corresponds to the minimum α energy. Because the penetration depth is much shorter than the distance in air, R_0 is very close to R. θ is the incident angle of α particles along the orange line in Figure 2. The depth S could be calculated by SRIM [36] with the parameter D and θ. S is the minimum detection depth on that etching condition (etching time, temperature) with PEW-25 solution and aluminum foil. For the laser-plasma experiment, the minimum
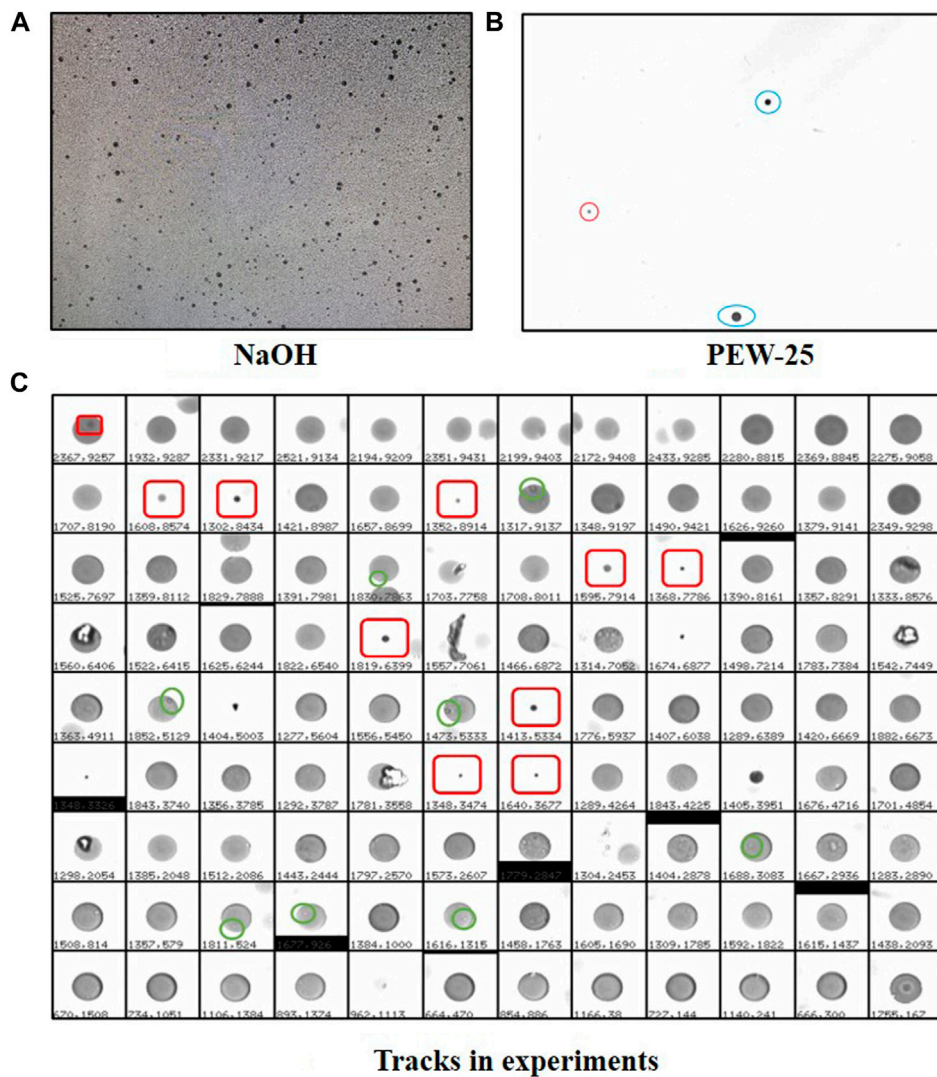
FIGURE 5
Surfaces of irradiated CR-39 after etching in the NaOH **(A)** and PEW-25 **(B)** solutions. The blue encircles tracks of ^{11}B or ^{12}C in **(B)**, and the red region is a track of α particles. **(C)** Tracks in the experiment with some tracks of α particle (red square). Tracks of heavier ions are much larger than those of α. The green circles in **(C)** indicate the overlapping of protons and ions.

vertically incident α energy can be estimated by the depth S. The minimum detection energy is 4.15 MeV after etching for 40 min in the PEW-25 solution at 60°C with 5.00 MeV α and 3.68 MeV for 30 min. An etch rate of 3.3 μm/10 min from the data can be estimated by E_{min} corresponding minimum depth S, which meets expectations as previously discussed.

Because the Bragg peak has a relatively slow climbing edge, as shown in Figure 1, the maximum α energy would span a wide range. Higher energy α particles leave a small track and a deeply grey level before they reach the Bragg peak, as shown in Figure 3I. These tracks would be present on CR-39 for a longer etching time. The diameter of the track gets larger and has a lower grey level as the etching time increases until the tracks disappear in the optical microscope. The maximum energy may be estimated by multiple etching times. Based on the experience of our calibration with different etching times and aluminum foils, we could roughly estimate the maximum energy in the range of 5.80 MeV ± 0.80 MeV for 40 min and 5.65 ± 0.60 MeV for 30 min.

In principle, one could etch the detector as many times as needed to increase the energy resolution. However, the temperature and concentration of the solution would change when the detector is taken out of and into the solution. Another problem is that the size of the α-particle track is around 8 μm which would cover a wide range of depth and result in a relatively bigger energy error. In our laser experiment, an etching time of 30 min was used. The etching procedure is applied for each detector since the covering with thick aluminum reduces the range of the α in the detectors.

3.4 Experimental results of irradiated CR-39 after etching in a solution

In our laser-induced nuclear reaction experiment, a PW laser pulse with a duration of 33 fs and an energy of 10–20 J in SIOM is used. CR-39 was irradiated with laser-accelerated protons, boron,
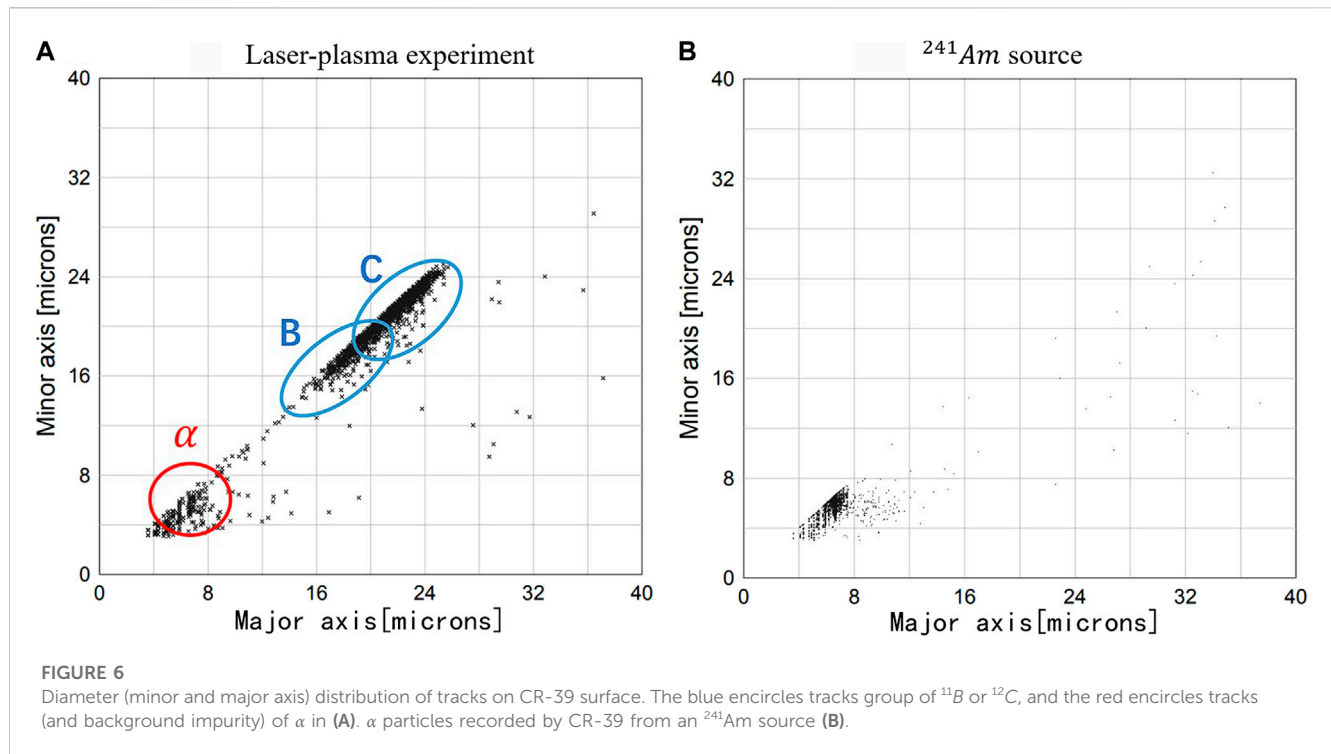
FIGURE 6
Diameter (minor and major axis) distribution of tracks on CR-39 surface. The blue encircles tracks group of ^{11}B or ^{12}C, and the red encircles tracks (and background impurity) of α in **(A)**. α particles recorded by CR-39 from an ^{241}Am source **(B)**.

TABLE 1 The correct number of α.

CR-39	Solid angle	Energy range	Detection efficiency
142	4.18×10^6	9.12×10^6	1.47×10^7

carbon, and small numbers of secondary alphas of interest. Figures 5A, B show photographs and microscopy images of the CR-39 etched in NaOH and PEW-25 solutions, respectively. The etch pits observed in Figure 5A were caused by indistinguishable α particles from the $p +^{11}B$ reaction and the laser-accelerated ions. Even TASLImage software could not record information, and the optical microscope could not focus on it. The tracks observed in Figure 5B may be produced by α particles and other heavy ions. The image is much cleaner, and α particles can be better distinguished from ions than when etched by NaOH solution. As shown in Figures 5C, 1, 6, the track diameter of heavier ions (e.g., boron and carbon) is much larger than α approximately three times. Interestingly, the LET of carbon is nearly three times greater than that of α. The diameter of tracks in CR-39 etched with PEW solution may have a positive linear correlation with the LET of ions.

The laser was focused to a 10-μm full width at half maximum (FWHM) focal spot with an F/4 off-axis parabola, reaching a peak intensity of 2×10^{20} W/cm^2 (a = 10) on a nanowire-array CH$_2$ + CB$_4$ target. The maximum number of α particles was measured to be 1.4×10^7. One shot with 142 α tracks was detected on CR-39. The distance between CR-39 and the target was 46 cm, corresponding to a solid angle of 2.34×10^{-4}. Assuming the experiment kinetic spectrum is the same as the theoretical one from a Geant4 simulation, one can estimate the number of α particles for this shot (Table 1).

We used EPOCH, a PIC (particle-in-cell) program [52, 53] combined with the reaction rate of $^{11}B(p, \alpha)2\alpha$ to simulate the experimental observation. The number of α particles was 2.4×10^7, slightly more than the number in our experiment result of CR-39 etching in the PEW-25 solution. As shown in Figure 5, not only α particles but ions with higher LET than the detection threshold can also be detected with a PEW-25 solution. It is a universal method for laser-plasma experiments to detect ions mixed with protons.

4 Conclusion and summary

In this study, a PEW solution was applied to raise the detection threshold of the CR-39 detector. We present calibration results for CR-39 detectors, which are widely used to discriminate ions in fusion reaction experiments, as CR-39 is insensitive to background EMP. Etching in the PEW solution effectively desensitizes the track sensitivity of CR-39. The combination of CR-39 and the PEW-25 etching solution [60˚C (17% KOH + 25%C$_2$H$_5$OH + 58%H$_2$O)] was successfully used to detect secondary α particles in the presence of a large number of primary protons and other energetic heavy ions. The α particles produced from the $^{11}B(p, \alpha)2\alpha$ reaction induced by ultra-intensity laser (pulse width of 30–40 fs, and energy of 10–20 J) were selectively detected by reducing the proton detection sensitivity of CR-39 with PEW-25 solution. The result confirms that CR-39 etched with a PEW-25 solution [37] has better discrimination of ions than that with a NaOH solution. The calibration offers various options for etching time, aluminum foil thickness, and α energy range. A 10-μm aluminum foil and 30 or 40 min etching time are suggested for the laser-induced $^{11}B(p, \alpha)2\alpha$ experiment. PEW solution can also be applied to detect the quantity of minor,

accelerated heavy ions in a laser-plasma environment with a large number of primary protons.

For higher energy alpha particles in other experiments, if CR39 is the suitable detector for the alpha (e.g., without Li), the PEW solution is still a useful method for identifying different particles. The maximum LET of alpha is stable with the higher energy alpha particles so that the tracks of alpha particles will not become large. Furthermore, it has no over-etching of PEW-25 with our calibration experiment. The alpha particle track will disappear quickly when the etching depth is longer than the location of the Bragg peak. Compared to the PEW, the NaOH solution will lead to an over-etching track of alpha, and the diameter of the 2–5 MeV alpha track can be up to 30 microns. For an alpha particle with energy up to 20 MeV [54], we believe the size of the alpha particle tracks remains smaller than heavier ions (using PEW), as long as the etching time is appropriate.

Data availability statement

The original contributions presented in the study are included in the article/Supplementary Material, further inquiries can be directed to the corresponding authors.

Author contributions

PW designed and performed the calibration of CR-39. He wrote the original draft of this paper and discussed it with all the authors for further improvement. He joined the laser-induced $^{11}B(p, \alpha)2\alpha$ experiment to collect α-particle data. XD contributed to the discussion of the calibration and the modification of the draft. He joined the laser-induced $^{11}B(p, \alpha)2\alpha$ experiment. ZM contributed to the discussion of the calibration and the modification of the draft. He joined the laser-induced $^{11}B(p, \alpha)2\alpha$ experiment. CF suggested the PEW solution for etching and provided the original reference work [37]. He also contributed to the discussion of the calibration and the modification of the draft. He joined the laser-induced $^{11}B(p, \alpha)2\alpha$ experiment. LF contributed to the discussion of the calibration and the modification of the draft. He joined the laser-induced $^{11}B(p, \alpha)2\alpha$ experiment. QW contributed to the discussion of the calibration and the modification of the draft. He joined the laser-induced $^{11}B(p, \alpha)2\alpha$ experiment. JX contributed to the discussion of the calibration and the modification of the draft. She led the laser-induced $^{11}B(p, \alpha)2\alpha$ experiment with GZ. TX contributed to the discussion of the calibration and the modification of the draft. He joined the laser-

induced $^{11}B(p, \alpha)2\alpha$ experiment. LJ contributed to the discussion of the calibration and the modification of the draft. BS contributed to the discussion of the calibration and the modification of the draft. YL contributed to the discussion of the calibration and the modification of the draft. He provided a professional chemistry laboratory for the etching of detectors. XC contributed to the discussion of the calibration and the modification of the draft. GZ proposed the idea for this work. He contributed to the preparation of the draft. He led the laser-induced $^{11}B(p, \alpha)2\alpha$ experiment with JX. YM is in charge of the project. He contributed to the modification of the draft $^{11}B(p, \alpha)2\alpha$ and joined the laser experiment. All authors contributed to the article and approved the submitted version.

Conflict of interest

The authors declare that the research was conducted in the absence of any commercial or financial relationships that could be construed as a potential conflict of interest.

Publisher's note

All claims expressed in this article are solely those of the authors and do not necessarily represent those of their affiliated organizations or those of the publisher, the editors, and the reviewers. Any product that may be evaluated in this article, or claim that may be made by its manufacturer, is not guaranteed or endorsed by the publisher.

References

1. Burbidge EM, Burbidge GR, Fowler WA, Hoyle F. Synthesis of the elements in stars. *Rev Mod Phys* (1957) 29:547–650. doi:10.1103/RevModPhys.29.547

2. Wallerstein G, Iben I, Parker P, Boesgaard AM, Hale GM, Champagne AE, et al. Synthesis of the elements in stars: Forty years of progress. *Rev Mod Phys* (1997) 69:995–1084. doi:10.1103/RevModPhys.69.995

3. Qian Y. Neutrinos, supernovae, and the origin of the heavy elements. *Sci China Phys Mech Astron* (2018) 61:049501. doi:10.1007/s11433-017-9142-2

4. Tang X-D, Ma S-B, Fang X, Bucher B, Alongi A, Cahillane C, et al. An efficient method for mapping the $c^{12} + c^{12}$ molecular resonances at low energies. *Nucl Sci Tech* (2019) 30:126. doi:10.1007/s41365-019-0652-9

5. Li Z, Niu Z, Sun B. Influence of nuclear physics inputs and astrophysical conditions on r-process. *Sci China Phys Mech Astron* (2019) 62:982011. doi:10.1007/s11433-018-9355-y

6. Liu H, Han D, Ma Y, Zhu L. Network structure of thermonuclear reactions in nuclear landscape. *Sci China Phys Mech Astron* (2020) 63:112062. doi:10.1007/s11433-020-1552-2

7. McKenna P, Ledingham KWD, McCanny T, Singhal RP, Spencer I, Santala MIK, et al. Demonstration of fusion-evaporation and direct-interaction nuclear reactions using high-intensity laser-plasma-accelerated ion beams. *Phys Rev Lett* (2003) 91:075006. doi:10.1103/PhysRevLett.91.075006

8. Belyaev VS, Matafonov AP, Vinogradov VI, Krainov VP, Lisitsa VS, Roussetski AS, et al. Observation of neutronless fusion reactions in picosecond laser plasmas. *Phys Rev E* (2005) 72:026406. doi:10.1103/PhysRevE.72.026406

9. Kong D, Zhang G, Shou Y, Xu S, Mei Z, Cao Z, et al. High-energy-density plasma in femtosecond-laser-irradiated nanowire-array targets for nuclear reactions. *Matter Radiat Extremes* (2022) 7:064403. doi:10.1063/5.0120845

10. Huang M, Quevedo HJ, Zhang G, Bonasera A. Nuclear astrophysics with lasers. *Nucl Phys News* (2019) 29:9–13. doi:10.1080/10619127.2019.1603555

11. Fu C, Zhang G, Ma Y. New opportunities for nuclear and atomic physics on the femto-to nanometer scale with ultra-high-intensity lasers. *Matter Radiat Extremes* (2022) 7:024201. doi:10.1063/5.0059405

12. Consoli F, De Angelis R, Andreoli P, Bonasera A, Cipriani M, Cristofari G, et al. Diagnostic methodologies of laser-initiated 11B(p,)2 fusion reactions. *Front Phys* (2020) 8:561492. doi:10.3389/fphy.2020.561492

13. Ren J, Deng Z, Qi W, Chen B, Ma B, Wang X, et al. Observation of a high degree of stopping for laser-accelerated intense proton beams in dense ionized matter. *Nat Commun* (2020) 11:5157. doi:10.1038/s41467-020-18986-5

14. Zhao YT, Zhang YN, Cheng R, He B, Liu CL, Zhou XM, et al. Benchmark experiment to prove the role of projectile excited states upon the ion stopping in plasmas. *Phys Rev Lett* (2021) 126:115001. doi:10.1103/PhysRevLett.126.115001

15. Margarone D, Morace A, Bonvalet J, Abe Y, Kantarelou V, Raffestin D, et al. Generation of -particle beams with a multi-kj, peta-watt class laser system. *Front Phys* (2020) 8. doi:10.3389/fphy.2020.00343

16. Margarone D, Bonvalet J, Giuffrida L, Morace A, Kantarelou V, Tosca M, et al. In-target proton–boron nuclear fusion using a pw-class laser. *Appl Sci* (2022) 12:1444. doi:10.3390/app12031444

17. Giuffrida L, Belloni F, Margarone D, Petringa G, Milluzzo G, Scuderi V, et al. High-current stream of energetic α particles from laser-driven proton-boron fusion. *Phys Rev E* (2020) 101:013204. doi:10.1103/PhysRevE.101.013204

18. Zhang G, Huang M, Bonasera A, Ma Y, Shen B, Wang H, et al. Nuclear probes of an out-of-equilibrium plasma at the highest compression. *Phys Lett A* (2019) 383: 2285–9. doi:10.1016/j.physleta.2019.04.048

19. Xi X, Zhang G, Liu F, Fu G, He C, Chen H, et al. Direct calibration of neutron detectors for laser-driven nuclear reaction experiments with a gated neutron source. *Rev Scientific Instr* (2023) 94:013301. doi:10.1063/5.0127101

20. Rubovič P, Bonasera A, Burian P, Cao Z, Fu C, Kong D, et al. Measurements of D–D fusion neutrons generated in nanowire array laser plasma using Timepix3 detector. *Nucl Instr Methods Phys Res Section A: Acc Spectrometers, Detectors Associated Equipment* (2021) 985:164680. doi:10.1016/j.nima.2020.164680

21. Bang W, Barbui M, Bonasera A, Dyer G, Quevedo HJ, Hagel K, et al. Temperature measurements of fusion plasmas produced by petawatt-laser-irradiated D₂-³He or CD₄-³He clustering gases. *Phys Rev Lett* (2013) 111:055002. doi:10.1103/PhysRevLett.111.055002

22. Barbui M, Bang W, Bonasera A, Hagel K, Schmidt K, Natowitz JB, et al. Measurement of the plasma astrophysical S factor for the 3He(d,p) 4He reaction in exploding molecular clusters. *Phys Rev Lett* (2013) 111:082502. doi:10.1103/PhysRevLett.111.082502

23. Hu P, Ma Z-G, Zhao K, Zhang G-Q, Fang D-Q, Wei B-R, et al. Development of gated fiber detectors for laser-induced strong electromagnetic pulse environments. *Nucl Sci Tech* (2021) 32:58. doi:10.1007/s41365-021-00898-8

24. Feng J, Wang W, Fu C, Chen L, Tan J, Li Y, et al. Femtosecond pumping of nuclear isomeric states by the coulomb collision of ions with quivering electrons. *Phys Rev Lett* (2022) 128:052501. doi:10.1103/PhysRevLett.128.052501

25. Nürnberg F, Schollmeier M, Brambrink E, Blažević A, Carroll DC, Flippo K, et al. Radiochromic film imaging spectroscopy of laser-accelerated proton beams. *Rev Scientific Instr* (2009) 80:033301. doi:10.1063/1.3086424

26. Meadowcroft AL, Bentley CD, Stott EN. Evaluation of the sensitivity and fading characteristics of an image plate system for x-ray diagnostics. *Rev Scientific Instr* (2008) 79:113102. doi:10.1063/1.3013123

27. Wang P, Gong Z, Lee SG, Shou Y, Geng Y, Jeon C, et al. Super-heavy ions acceleration driven by ultrashort laser pulses at ultrahigh intensity. *Phys Rev X* (2021) 11:021049. Publisher: APS. doi:10.48550/arXiv.2008.09358

28. Boutoux G, Rabhi N, Batani D, Binet A, Ducret J-E, Jakubowska K, et al. Study of imaging plate detector sensitivity to 5-18 mev electrons. *Rev Scientific Instr* (2015) 86: 113304. doi:10.1063/1.4936141

29. Boutoux G, Batani D, Burgy F, Ducret J, Forestier-Colleoni P, Hulin S, et al. Validation of modelled imaging plates sensitivity to 1-100 kev x-rays and spatial resolution characterisation for diagnostics for the " petawatt aquitaine laser. *Rev Scientific Instr* (2016) 87:043108. doi:10.1063/1.4944863

30. Fleischer RL, Price PB, Walker RM, Hubbard EL. Criterion for registration in dielectric track detectors. *Phys Rev* (1967) 156:353–5. doi:10.1103/PhysRev.156.353

31. Barillon R, Fromm M, Chambaudet A, Marah H, Sabir A. Track etch velocity study in a radon detector (lr 115, cellulose nitrate). *Radiat Measurements* (1997) 28: 619–28. International Conference on Nuclear Tracks in Solids. doi:10.1016/S1350-4487(97)00153-4

32. Cartwright B, Shirk E, Price P. A nuclear-track-recording polymer of unique sensitivity and resolution. *Nucl Instr Methods* (1978) 153:457–60. doi:10.1016/0029-554X(78)90989-8

33. Guo S-L, Chen B-L, Durrani S. Chapter 3 - solid-state nuclear track detectors. In: MF L'Annunziata editor. *Handbook of radioactivity analysis*. 4th ed. United States: Academic Press (2020). p. 307–407. doi:10.1016/B978-0-12-814397-1.00003-0

34. Rana MA. Thermodynamics of nuclear track chemical etching. *Nucl Instr Methods Phys Res Section A: Acc Spectrometers, Detectors Associated Equipment* (2018) 890: 68–71. doi:10.1016/j.nima.2018.02.041

35. Sadowski M, Al-Mashhadani E, Szydłowski A, Czyzewski T, Głowacka L, Jaskóła M, et al. Comparison of responses of CR-39 and PM-355 track detectors to fast protons, deuterons and 4he ions within energy range 0.2–4.5 MeV. *Radiat Measurements* (1995) 25:175–6. doi:10.1016/1350-4487(95)00066-N

36. Ziegler JF. Srim-2003. *Nucl Instr Methods Phys Res Section B: Beam Interactions Mater Atoms* (2004) 219-220:1027–36. Proceedings of the Sixteenth International Conference on Ion Beam Analysis. doi:10.1016/j.nimb.2004.01.208

37. Nishiura Y, Inoue S, Kojima S, Teramoto K, Furukawa Y, Hashida M, et al. Detection of alpha particles from ⁷ li(p,α) ⁴ he and ¹⁹ f(p,α) ¹⁶ o reactions induced by laser-accelerated protons using CR-39 with potassium hydroxide–ethanol–water etching solution. *Rev Scientific Instr* (2019) 90:083307. doi:10.1063/1.5098863

38. Rana MA, Qureshi I. Studies of CR-39 etch rates. *Nucl Instr Methods Phys Res Section B: Beam Interactions Mater Atoms* (2002) 198:129–34. doi:10.1016/S0168-583X(02)01526-4

39. Awad EM, Rana MA, Al-Jubbori MA. Bulk etch rates of CR-39 at high etchant concentrations: Diffusion-limited etching. *Nucl Sci Tech* (2020) 31:118. doi:10.1007/s41365-020-00830-6

40. He Y-F, Xi X-F, Guo S-L, Guo B, He C-Y, Liu F-L, et al. Calibration of CR-39 solid-state track detectors for study of laser-driven nuclear reactions. *Nucl Sci Tech* (2020) 31: 42. doi:10.1007/s41365-020-0749-1

41. Zhang Y, Wang H-W, Ma Y-G, Liu L-X, Cao X-G, Fan G-T, et al. Energy calibration of a CR-39 nuclear-track detector irradiated by charged particles. *Nucl Sci Tech* (2019) 30:87. doi:10.1007/s41365-019-0619-x

42. Soares C, Alencar I, Guedes S, Takizawa R, Smilgys B, Hadler J. Alpha spectrometry study on lr 115 and makrofol through measurements of track diameter. *Radiat Measurements* (2013) 50:246–8. doi:10.1016/j.radmeas.2012.06.010

43. Hermsdorf D. Evaluation of the sensitivity function V for registration of α-particles in PADC CR-39 solid state nuclear track detector material. *Radiat Measurements* (2009) 44:283–8. doi:10.1016/j.radmeas.2009.03.028

44. Hermsdorf D. Physics aspects of light particle registration in PADC detectors of type CR-39. *Radiat Measurements* (2011) 46:396–404. doi:10.1016/j.radmeas.2011.02.012

45. Rana MA. Summary of a comprehensive data bank for nuclear track research using CR-39 detectors. *Nucl Instr Methods Phys Res Section A: Acc Spectrometers, Detectors Associated Equipment* (2019) 944:162590. doi:10.1016/j.nima.2019.162590

46. Oliveira C, Malheiros B, Pires K, Assunção M, Guedes S, Corrêa J, et al. Low energy alpha particle tracks in CR-39 nuclear track detectors: Chemical etching studies. *Nucl Instr Methods Phys Res Section A: Acc Spectrometers, Detectors Associated Equipment* (2021) 995:165130. doi:10.1016/j.nima.2021.165130

47. Kodaira S, Aasaeda M, Doke T, Hareyama M, Hasebe N, Ogura K, et al. Track detector of CR-39-DAP-copolymer with variable threshold to detect trans-iron nuclei in galactic cosmic rays. *Radiat Measurements* (2008) 43:S52–5. doi:10.1016/j.radmeas.2008.03.052

48. Kodaira S, Yasuda N, Kawashima H, Kurano M, Hasebe N, Doke T, et al. Characteristics of the copolymerized CR-39/DAP track detector for the observation of ultra heavy nuclei in galactic cosmic rays. *Radiat Measurements* (2009) 44:775–8. doi:10.1016/j.radmeas.2009.10.050

49. Yanagie H, Ogura K, Matsumoto T, Eriguchi M, Kobayashi H. Neutron capture autoradiographic determination of distributions and concentrations in biological samples for boron neutron capture therapy. *Nucl Instr Methods Phys Res Section A: Acc Spectrometers, Detectors Associated Equipment* (1999) 424:122–8. doi:10.1016/S0168-9002(98)01284-4

50. Kodaira S, Yasuda N, Kawashima H, Kurano M, Hasebe N, Doke T, et al. Control of the detection threshold of CR-39 PNTD for measuring ultra heavy nuclei in galactic cosmic rays. *Radiat Measurements* (2009) 44:861–4. doi:10.1016/j.radmeas.2009.10.057

51. Somogyi G, Hunyadi I. Etching properties of the CR-39 polymeric nuclear track detector. *Solid State Nucl Track Detectors* (1980) 1980:443. doi:10.1016/B978-0-08-025029-8.50055-X

52. Arber TD, Bennett K, Brady CS, Lawrence-Douglas A, Ramsay MG, Sircombe NJ, et al. Contemporary particle-in-cell approach to laser-plasma modelling. *Plasma Phys Controlled Fusion* (2015) 57:113001. doi:10.1088/0741-3335/57/11/113001

53. Derouillat J, Beck A, Perez F, Vinci T, Chiaramello M, Grassi A, et al. Smilei: A collaborative, open-source, multi-purpose particle-in-cell code for plasma simulation. *Comput Phys Commun* (2018) 222:351–73. doi:10.1016/j.cpc.2017.09.024

54. Bonvalet J, Nicolaï P, Raffestin D, D'Humières E, Batani D, Kantarelou V, et al. Energetic -particle sources produced through proton-boron reactions by high-energy high-intensity laser beams. *Phys Rev E, Stat Phys Plasmas Fluids Relat Interdiscip Top* (2021) 103:053202. doi:10.1103/PhysRevE.103.053202